Measurement of ^{235}U$(n, n'\gamma)$ and ^{235}U$(n, 2n\gamma)$ reaction cross sections

M. Kerveno,[1,*] J. C. Thiry,[1] A. Bacquias,[1] C. Borcea,[2] P. Dessagne,[1] J. C. Drohé,[3] S. Goriely,[4] S. Hilaire,[5] E. Jericha,[6] H. Karam,[1] A. Negret,[2] A. Pavlik,[7] A. J. M. Plompen,[3] P. Romain,[5] C. Rouki,[3] G. Rudolf,[1] and M. Stanoiu[2]

[1]*CNRS, Université de Strasbourg, UMR7178, IPHC, 23 Rue du Loess, 67037 Strasbourg, France*

[2]*National Institute of Physics and Nuclear Engineering "Horia Hulubei", Reactorului 30, 077125 Bucharest-Magurele, Romania*

[3]*European Commission, Joint Research Centre, Institute for Reference Materials and Measurements, Retieseweg 111, B-2440 Geel, Belgium*

[4]*Institut d'Astronomie et d'Astrophysique, CP-226, Université Libre de Bruxelles, BE-1050 Brussels, Belgium*

[5]*CEA, DAM, DIF, F-91297 Arpajon, France*

[6]*Technische Universität Wien, Atominstitut, Stadionallee 2, 1020 Wien, Austria*

[7]*University of Vienna, Faculty of Physics, Währinger Straße 17, 1090 Wien, Austria*

(Received 13 November 2012; revised manuscript received 20 December 2012; published 22 February 2013)

The design of generation IV nuclear reactors and the studies of new fuel cycles require knowledge of the cross sections of various nuclear reactions. Our research is focused on $(n, xn\gamma)$ reactions occurring in these new reactors. The aim is to measure unknown cross sections and to reduce the uncertainty on present data for reactions and isotopes of interest for transmutation or advanced reactors. The present work studies the ^{235}U$(n, n'\gamma)$ and ^{235}U$(n, 2n\gamma)$ reactions in the fast neutron energy domain (up to 20 MeV). The experiments were performed with the Geel electron linear accelerator GELINA, which delivers a pulsed white neutron beam. The time characteristics enable measuring neutron energies with the time-of-flight (TOF) technique. The neutron induced reactions [in this case inelastic scattering and $(n, 2n)$ reactions] are identified by on-line prompt γ spectroscopy with an experimental setup including four high-purity germanium (HPGe) detectors. A fission ionization chamber is used to monitor the incident neutron flux. The experimental setup and analysis methods are presented and the model calculations performed with the TALYS-1.2 code are discussed.

DOI: 10.1103/PhysRevC.87.024609 PACS number(s): 25.40.Fq, 24.10.−i, 28.20.Cz, 29.30.Kv

I. INTRODUCTION

Nuclear reactors currently in operation are mainly based on the use of the fissile ^{235}U isotope as fuel. While ^{235}U is predicted to become scarce within the next 50 years, new reactor types are being developed in order to make use of fertile material, which is transformed to fissile material following neutron capture. On another issue, current reactor research deals with new systems, able to reduce the radiotoxicity of nuclear waste through transmutation or incineration. An important initiative for the study of such advanced reactors is the Generation-IV International Forum [1].

A large number of these possible future reactors are operated with a fast neutron spectrum, versus thermal neutrons in the present reactors. With the higher kinetic energy of neutrons present in the core, new reaction channels open, that are not well quantified at this stage. Of particular importance are (n, xn) reactions.

Indeed, precise knowledge of these reactions is a key issue in present day reactor development studies. They are crucial for the design of new reactors as they represent an important energy loss mechanism which has to be taken into account in the calculations. In addition, they lead to neutron multiplication and production of radioactive isotopes, affecting reactor neutron economy and transport as well as radiation shielding. For this reason target uncertainties for important reactor parameters have been converted to reaction cross section target uncertainties, requiring precision of 5% and better for numerous isotopes of interest [2–5].

Several techniques may be used to measure (n, xn) reactions. In general, none of the methods is perfect and the information they provide is complementary. The measurement of (n, xn) reactions on long-lived, fissionable actinides is very delicate, as some of the measurement techniques are very difficult to apply here. For the activation method the irradiation and measurement time have to be a reasonable fraction of the half-life of the produced isotopes when decay radiation is used for the determination of the activity, often leading to long measurement and irradiation times. In addition the produced activity should be significantly larger than the activity of the product isotope in the sample prior to irradiation. Only in favorable cases can these problems be overcome by the use of accelerator mass spectrometry, and this does not apply to the case of study here: ^{235}U.

Another method is the measurement of secondary neutrons, which has the disadvantage that it is not straightforward to distinguish between neutrons coming from elastic scattering, inelastic scattering, or $(n, 2n)$ reactions in the overlapping regions. The situation is even more complicated for fissionable isotopes, for which additional neutrons are produced due to neutron induced fission. Moreover, the angular distribution of the neutrons depends strongly on the reaction mechanism, and has to be measured over the complete angular range.

For these reasons, the prompt γ-ray spectroscopy method was chosen for the experiments in the present work. With this measurement technique a sample is bombarded by a unidirectional neutron beam and the emitted γ radiation accompanying

*maelle.kerveno@iphc.cnrs.fr

neutron emission in (n, xn) reactions is measured. This method was already used at the Karlsruhe isochronous cyclotron for the study of isotopes such as ^{27}Al, ^{56}Fe, and also ^{238}U [6] in the 1970s. In the 90s, it was also used at the ORELA facility to study $(n, xn\gamma)$ reactions on Cr, Fe, and other isotopes [7]. More recently, at the Los Alamos National Laboratory, $(n, xn\gamma)$ reaction measurements on ^{207,208}Pb [8] and later also other isotopes such as ^{239}Pu [9] were performed.

The present work was realized at the white, pulsed neutron beam facility of the Geel Linear Accelerator (GELINA) of the Institute for Reference Materials and Measurements (IRMM), Belgium. As low uncertainties on the measured data were of crucial importance in this work, great care was taken in the design of the experimental setup and on the determination of the efficiencies of the employed detectors.

The results are compared to nuclear model codes, such as TALYS-1.2 [10], in order to verify the level density models and branching ratios, which are fundamental for the prediction of γ-ray productions. Measurements of $(n, xn\gamma)$ reaction cross sections can give new insight in these different parameters by providing stronger constraints and thus improve the ability of theoretical codes to predict nuclear reactions.

II. EXPERIMENTAL SETUP

The experimental setup used for the measurements in this work is shown in Fig. 1. The neutron beam produced by the GELINA facility is impinging on a enriched uranium 235 sample. Following (n, xn) reactions, the nucleus is left in an excited state, decaying by γ-ray emission. These rays, characteristic of the produced nucleus, and thus of the reaction in question, are measured using four high-purity germanium (HPGe) detectors, referred to as grey, red, green, and blue. They are placed around the target at well defined angles, in order to take into account the angular distribution of the γ emission. The incident neutron flux is monitored using a fission ionization chamber, mounted upstream of the sample.

A. Neutron beam delivered by GELINA

GELINA is a multiuser neutron time-of-flight (TOF) facility in Geel, Belgium [11,12]. Neutrons are produced by

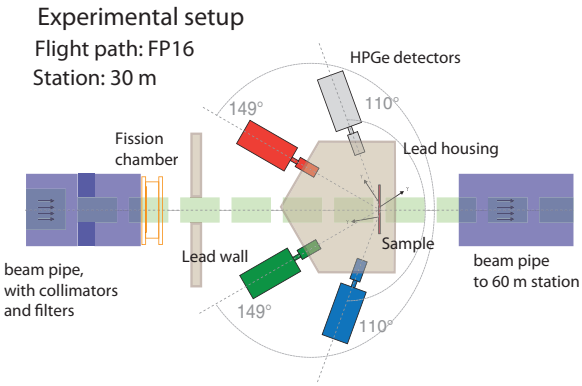

FIG. 1. (Color online) Experimental setup used for the measurements in this work.

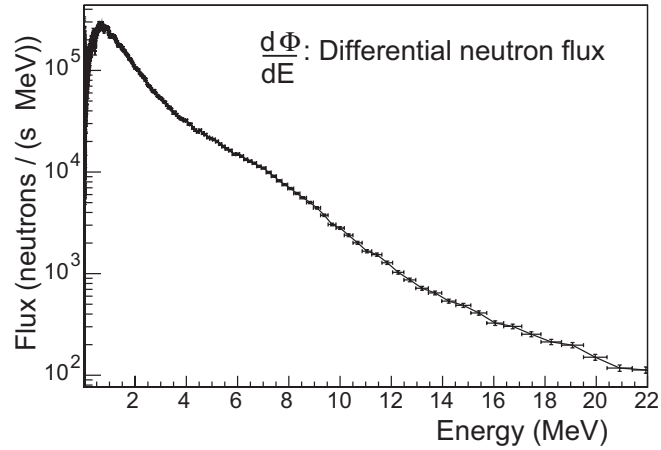

FIG. 2. Differential neutron flux measured at FP16/30m at GELINA.

electrons from the linear accelerator hitting a uranium target. The generated beam presents a combined evaporation and fission spectrum, peaking at 2 MeV and producing neutrons up to 20 MeV, but its intensity decreases quickly with increasing neutron energy, as shown in Fig. 2. For the experiments in this work, the accelerator was operated at a repetition rate of 800 Hz.

The neutrons emitted from the production target are collimated into 12 flight paths, where experiments can be carried out at different flight distances. Specific filters are introduced into the beam in order to absorb undesirable radiation: first, a depleted uranium filter of 52.8 g/cm^2 very close to the neutron source is used in order to reduce the intensity of the γ flash (remaining bremsstrahlung γ rays from the primary neutron production target, arriving at the measurement stations just before the neutrons). Additionally, ^{10}B filters with a total thickness of 760 mg/cm^2 cut out slow and thermal neutrons, overlapping with neutrons of the following bursts. The diameter of the neutron beam in this work was 55 mm.

Thanks to the presence of a compression magnet [13], the time resolution of the beam is less than 1 ns full width at half maximum (FWHM), allowing precise time-of-flight measurements, and hence a good neutron energy determination. Our measurements are realized at a flight station located 30 m away from the neutron source. The data acquisition resolution being 10 ns, this flight path is the best compromise between time resolution and flux intensity, allowing a resolution of 1 MeV at a neutron energy of 20 MeV.

Different noise and background sources present at the GELINA facility were analyzed, and special care was taken in the conception of the experimental setup in order to reduce their effects to a minimum. On one side, the powerful modulators of the linear electron accelerator generate a considerable electromagnetic noise, resulting in pulse distortion of the HPGe signals. For this reason the setup grounding was strongly enhanced, and only triple-shielded cables in conjunction with ferrite (cutting out the high-frequency noise) were used in the connections of the detectors to the data acquisition system. On the other side, a considerable γ radiation background is created, through scattering of the remaining Bremsstrahlung

TABLE I. Technical specifications and distances to the sample of the four HPGe detectors used in the experiment. Values are in mm.

Detector	Distance to sample	Ge diameter	Ge thickness
Grey	167.6(5)	58.0(2)	30.0(2)
Red	218.7(5)	59.0(2)	27.5(2)
Green	141.0(5)	34.8(2)	20.0(2)
Blue	134.6(5)	35.1(2)	19.6(2)

γ rays from the primary neutron target, on the other flight paths close to our station. In order to reduce the detection of these to a minimum, the sample together with the front of the semiconductor detectors were shielded by a lead construction made from 50 mm thick bricks, and the fronts of the detectors were protected by an additional copper cylinder.

B. HPGe detectors

The γ rays emitted following the ^{235}U(n, xn) reactions are detected using four HPGe counters, made of semi-planar crystals with depths ranging from 2 to 3 cm and surfaces dimensioned between 10 and 28 cm^2. Their specifications and distances to the sample are given in Table I. The crystals are optimized for high-resolution detection at low energies (resolution of 0.7 keV at 122 keV). They are placed at angles of 110° and 149° which allows the angular dependence to be taken into account. Backward angles were chosen to reduce dead time caused by the observation of events due to γ flash scattering, affecting up to 50% of the counts, depending on the detector position and size.

As the beam, and hence the ^{235}U sample used (see Sec. II D), is not point-like and as the self-absorption coefficient in such dense materials is rather high, the efficiency of the HPGe detectors was calculated using a GEANT4 [14] simulation code, which is verified through measurements with calibrated sources [15]. The procedure for this method is realized in several steps: first, the geometry of the crystal is determined and entered into a GEANT4 simulation code. For this purpose, the detectors were characterized precisely by computed tomography at the microfocus computer tomography device of the Department of Metallurgy and Materials Engineering (MTM) at the Katholieke Universiteit Leuven (KUL). A polychromatic x-ray source (Philips HOMX 161) operated at a voltage of 125 kV and a current of 0.28 mA filtered by a 2 mm aluminium and a 1 mm copper shield [16] allowed a detector scan at a precision of approximately 100–200 μm.

In a second step, calibrated sources are used: for this work, point-like ^{152}Eu and ^{133}Ba sources (placed at different spots of the sample position) and an extended ^{152}Eu source were employed. The obtained results are compared to the simulated spectra. The observed differences in the yields are used to determine the dead layers of the crystal and to fix the simulation input. Once the simulation parameters are set, the third step consists of simulating the studied sample. For this purpose the geometry of the sample is entered into the simulation code and the origins and the directions of the γ rays emitted from the sample with specific energies are sampled randomly. The ratio between the number of events in the photo-peak and the number of γ rays simulated is the absolute peak efficiency of the detector. The efficiency results obtained hereby were verified by similar simulations using the MCNPX [17] calculation code, and a very good agreement was found.

With this technique the detection efficiency of the detectors could be determined at a precision ranging between 2% and 3% in the energy domain of interest. A more detailed description of the efforts made to reduce the uncertainty on the detection efficiency is given in Refs. [18,19]

C. Fission chamber

The precision of cross section measurements depends very strongly on the uncertainties of the incident neutron flux (Fig. 2), thus it is of uppermost importance to have very precise flux data.

The flux is measured using a ^{235}U fission ionization chamber. The deposit, highly enriched in ^{235}U (>99.5%) is made of a vacuum evaporated $^{235}UF_4$ layer which is very thin [324(2) μg/cm^2]. Despite its small thickness, some fission fragments are absorbed inside the layer itself. In order to take these losses into account, several corrections are applied to the counted fragments in the ionization chamber as elaborated in detail by Budtz-Jørgensen *et al.* [20] for thermal neutrons. Moreover, a further correction is made for anisotropies of the fission product angular distributions for kinetic effects as described by Carlson *et al.* [21].

Another aspect present in the determination of the efficiency of the fission ionization chamber to detect a fission fragment is the method used to subtract the α particle signals, stemming from the radioactivity of the uranium layer. In this work, the elimination of these events is realized through the application of an energy threshold above the maximum α-particle energy. For this purpose, the fission chamber's design, namely the thickness of the ionization chamber and the application of forward or reverse biasing, was studied in order to reduce the losses through application of a threshold. The chosen configuration consists in a thickness of 6 mm for the active detection volume, and a forward bias application.

The correction for fission fragment events cut out by the threshold method are determined via linear extrapolation of the fission fragment plateau to zero energy [22]. The above corrections result in an efficiency varying between 93% and 95%, depending on the neutron energy, to be applied to the counted events above the α-particle rejection threshold [18,19].

In order to verify these calculations, the fission chamber was calibrated using a monoenergetic ($E = 8.4$ MeV) neutron beam produced at the Physikalisch Technische Bundesanstalt (PTB) in Braunschweig through ^{2}H$(d, n)^3$He reactions on a gas target. The beam was well characterized by different reference measurements of high precision, including a recoil proton telescope (RPT), a liquid scintillation detector, and fission chambers with ^{235}U and ^{238}U layers [23]. Time-of-flight and energy information were saved in list mode files, enabling time gating on the acquired data, to eliminate neutrons with wrong energy, e.g., born through breakup reactions in the deuterium target or slowed down through scattering in the

experimental hall. For the measurements several foreground runs were performed to obtain statistics of at least 10 000 events in the fission chamber. Two series of background measurements were made: the first by placing a shadow cone between the neutron source and the detector to evaluate the indirect component of fission events generated, and a second by taking the deuterium gas out of the target cell and bombarding the empty target with deuteron particles to estimate the amount of neutrons created by mechanisms outside the deuterium gas volume.

After corrections for acquisition dead time and air attenuation, these measurements enabled us to determine the efficiency to detect a fission event in the ionization chamber to be (94.4 ± 2.1)% at an incident neutron energy of 8.4 MeV. This value is in excellent agreement with the calculation mentioned above, for which the efficiency calculations yield the same value at the given neutron energy.

D. Uranium sample

As uranium is very dense, thick samples would strongly absorb emitted γ rays which are to be detected and hence lead to an important correction factor due to self-absorption inside the target. Another problem of uranium is its radioactivity causing dead time on the data acquisition system while also limiting statistical accuracy through background and the ability to resolve γ rays of interest.

For these reasons, it is preferable to use thin layers: the chosen sample has a thickness of 0.211 mm with an uncertainty of 0.006 mm. The error on the thickness corresponds to the standard deviation obtained on a set of 18 measurements at different spots of the deposit. The sample is circular with a diameter of 120 mm. As the beam diameter is only 55 mm, the outer part of this source has been shielded with lead to reduce counting rates caused by the natural radioactivity of uranium. Further specifications are given in Table II.

These specifications yield an apparent density of the sample of 15.67 g/cm^3, whereas the theoretical density for natural uranium is 18.9 g/cm^3. This reveals that the sample suffers from oxidation. With a surface oxidation of a UO_2 [24] layer of density 10.97 g/cm^3, we suppose the sample to be a mix of pure uranium metal (enriched to 93.2%) and a UO_2 surface composite. These observations lead to a pure uranium mass of 36.2 g and an areal density of 0.320(4) g/cm^2. The uncertainty on this last quantity has been evaluated to take into account the lack of accuracy concerning the determination of uranium mass in the sample and the knowledge of the chemical form and physical structure of the oxide.

In order to study the effect of the penetration depth of the UO_2 on the γ-ray self-absorption inside the uranium target, different scenarios were tested. The difference between the two extreme considerations of a sample with a uniform density of 15.67 g/cm^3, and a sample with pure metal uranium in the center between a UO_2 sandwich were of the order of 2%. This additional uncertainty is added to the detection efficiency uncertainty.

TABLE II. Specifications of the ^{235}U sample used for the experiments.

^{235}U enrichment	93.20(3)	%
Total mass	37.43(1)	g
Diameter	12.004(4)	cm
Thickness	0.211(6)	mm (std. dev.)

TABLE III. Calculated differences between cross sections in the case of UO_2 and U_3O_8 surface oxidation consideration for the four analyzed γ transitions.

E_γ (keV)	129.3	152.7	201.0	244.2
$\frac{\sigma_{UO_2}(n,xn\gamma)}{\sigma_{U_3O_8}(n,xn\gamma)} - 1$	3.412%	2.321%	1.177%	1.116%

Moreover, the case of a surface oxidation with formation of a U_3O_8 deposit has been also studied. This hypothesis leads to a pure uranium mass of 36.5 g and an areal density of 0.323(4) g/cm^2. The effect of the two different oxidation considerations on the cross section calculations are reported in Table III.

In this work, we have chosen to consider a UO_2 surface oxidation.

E. Data acquisition

The signals arising from the detectors (HPGe and fission chamber) are processed by TNT2 (Treatment for NTof) [25] cards developed at the Institut Pluridisciplinaire Hubert Curien (IPHC). Signals are processed online in parallel in two different channels, one determining the event time by applying the constant fraction discriminator (CFD) method and one calculating the γ-ray energy of the incident events using the Jordanov [26] signal treatment method. The events are stored in list mode files, where the energy is encoded on 14 bits and the time step is 10 ns.

III. DATA ANALYSIS

This section describes the different steps followed in the data analysis to get from the acquired data to the final cross sections. During the entire experiment, the HPGe detectors were operated together with the fission ionization chamber, in order to monitor the incident neutron flux precisely for the entire run time.

A. γ-ray counting

The first part of the analysis consists in treating the acquired list mode files and choosing an appropriate time binning for which γ energy spectra are then generated. Depending on the counting statistics of events of interest, the choice of this binning is a compromise between a sufficient number of counts per bin to reduce the error on the counting and the best time of flight and thus neutron energy resolution. The chosen time binning depends on the strengths of the studied γ-ray production cross sections and on the incident neutron flux.

Once the binning is chosen, the number of hits detected in each peak n_{GE} is determined via integration, subtraction of the background, and correction for data acquisition dead time.

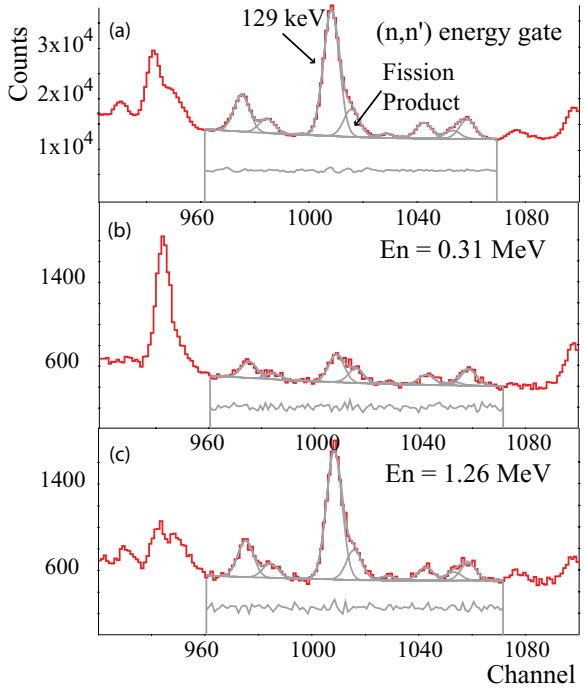

FIG. 3. (Color online) Example of the use of the GF3 software for the γ-ray fit procedure in the case of contamination in a peak (case of the 129.3 keV gamma transition in ^{235}U). (a) The fit obtained for the total (n, n') energy range for which the parameters of the fit are obtained. They are then used for fitting the peaks in each neutron energy bin as is shown for $E_n = 0.31$ MeV (b) and $E_n = 1.26$ MeV (c). The energy calibration is E_γ (keV) $= 0.128 \times$ channel $+ 0.186$.

The GF3 software [27] is used for the fitting procedure. An example is shown in Fig. 3 for the case of the 129.3 keV γ-ray transition in ^{235}U which is contaminated by a γ ray probably emitted by a fission product (see Sec. IV A1). The parameters (peak position, FWHM) of the fitting procedure are determined in the total (n, n') energy range [Fig. 3(a)] and then used to fit the peaks for all time gated γ energy spectra [see Figs. 3(b) and 3(c), corresponding to two neutron energy gates].

B. Dead-time correction

The digital data acquisition setup presents a dead time of around 4 μs, which corresponds to the time needed for one detected event to be treated properly. When a second event occurs during this time gap, both events cannot be distinguished and are then lost. For this reason, a decay γ ray emitted by the highly radioactive sample used in the experiment is monitored constantly to obtain precise time-of-flight dependent dead-time information.

Figure 4(a) shows a raw time spectrum, i.e., without pileup events. The drop in the count yield caused by the γ flash can be clearly observed starting 4 μs before the flash and extending to 4 μs after. Figure 4(b) shows the correction factor λ for the spectra obtained by monitoring the 185.7 keV γ ray coming from the radioactivity decay of the ^{231}Th isotope created after an α emission from ^{235}U.

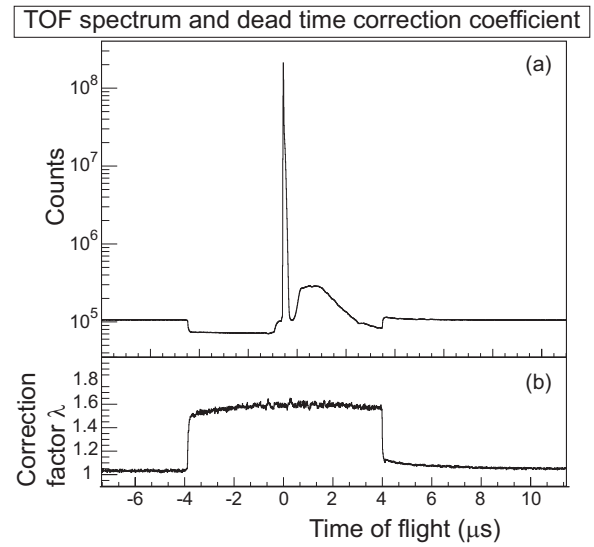

FIG. 4. Raw time-of-flight spectrum where no pileup events are considered for the green detector (a), and correction factor λ as a function of time for the dead time and pileup correction (b).

The correction factor at the beginning of the time gate equals roughly 1.03, caused by a 3% dead time measured for constant radioactivity counting. Upon the arrival of the γ flash, however, one can observe a correction of $\lambda > 1.6$. The γ flash is thus the main factor creating dead time, in this case around 60% for the green detector.

C. Incident neutron flux determination

As mentioned earlier, the incident neutron flux is determined with a fission chamber, mounted upstream of the uranium sample in the neutron flight path. Similarly as for the HPGe detectors, the acquired data is binned on the time-of-flight spectrum in order to obtain an energy-dependent flux. For these time bins, the pulse height spectra are integrated above the α-particle rejection threshold to obtain the number of detected fission fragments. As the neutron flux is not supposed to have much structure, these bins can be chosen large enough to obtain a high number of events and thus reduce the statistical error.

Unlike in the HPGe detectors, the γ flash does not generate many events in the fission chamber. For this reason the dead time is mostly due to the α particles following from the radioactive decay of the ^{235}U layer, and a constant correction factor can be applied.

As the flight distance to the fission chamber is different from the distance to the sample, we compute the differential number of hits $\frac{dn_{\text{det}}}{dE}$. This quantity is then integrated over the time bins chosen on the γ spectra to obtain the exact flux for the selected binning.

After the calculation of the neutron yield, one more correction has to be considered. As the flux is measured 1.56 m upstream of the sample, the neutrons counted in the fission chamber will subsequently suffer from attenuation in the remaining part of the fission chamber, but mostly in the air before the sample. To take these effects into account, MCNPX

simulations were performed and a mean attenuation of 1.8% was found and used as correction factor of the effective neutron yield hitting the sample.

D. Differential cross sections

In this work, we have measured the differential production cross section for γ transitions of interest, which means the data are not corrected for the internal conversion process. At a given angle θ_i and neutron energy E_n, the differential production cross section can be expressed as

$$\frac{d\sigma}{d\Omega}(\theta_i, E_n) = \frac{1}{4\pi}\frac{n_{GE}(\theta_i, E_n)}{n_{FC}(E_n)}\frac{\varepsilon_{FC}}{\varepsilon_{GE}}\frac{\varsigma_{FC}}{\varsigma_{sple}}\sigma_F(E_n), \qquad (1)$$

where n_{GE} and n_{FC} represent the dead-time corrected numbers of counts for a given γ ray in the HPGe energy spectrum and for the fission chamber counts above the discrimination threshold respectively, ε_{GE} and ε_{FC} the Germanium detector's and the fission chamber's efficiency, σ_F the ^{235}U fission cross section, and ς_{FC} and ς_{sple} the areal density (atoms/cm^2) of target nuclei in the fission chamber and in the sample.

E. Angle integration

The quantity of interest is the total reaction cross section, which requires integration of Eq. (1). One can show that the differential cross section can be expressed as a finite sum over even degree Legendre polynomials:

$$\frac{d\sigma}{d\Omega}(\theta) = \frac{\sigma_{\text{tot}}}{4\pi}\sum_{i=0}^{M}\alpha_i P_i(\cos\theta), \qquad (2)$$

where σ_{tot} is the total angle integrated cross section, and the α_i are coefficients ($\alpha_0 = 1$) depending on the angular momentum of the initial and final states J_i, J_f. The highest order Legendre polynomial in the decay distribution has order $\leqslant 2L$ and $\leqslant 2J_i$, where L is the largest multipolarity of importance for the transition, hence limiting this summation to M terms, where $M = \min\{2L, 2J_i\}$.

For transitions of states of well defined parity, the sum can be limited to even Legendre polynomials up to the order of 6 as the contribution of higher-order polynomials is small, reflecting the fact that there are few transitions with mixed multipolarities greater than 3. For multipolarities less than or equal to 3 the method of integration is exact for point sources and point detectors. Finite sample or detector size effects are negligible in the present arrangement. Under this assumption the integrated cross section can be obtained in very good approximation from measurements at only two angles where the value of the fourth-order Legendre polynomial P_4 is zero, leading to

$$\sigma_{tot} \approx 4\pi\left[w_1^*\frac{\mathrm{d}\sigma}{\mathrm{d}\Omega}(\theta_1^*) + w_2^*\frac{\mathrm{d}\sigma}{\mathrm{d}\Omega}(\theta_2^*)\right] \qquad (3)$$

with $\theta_1^* = (30.6^\circ \text{ or } 149.4^\circ)$, $\theta_2^* = (70.1^\circ \text{ or } 109.9^\circ)$, $w_1^* = 0.3479$, and $w_2^* = 0.6521$ for the zeros of P_4 [28–31].

F. Uncertainties

The uncertainties on the measured cross sections have been computed using the well known propagation of uncertainty formulas. The optimization of the experimental setup led to uncertainties on the efficiency parameters of 2.1% on ε_{FC} and 2% to 3% on the different Germanium detectors' efficiencies ε_{Ge}. The areal densities of the sample and the uranium layer in the fission chamber are known at respectively 1.2% and 0.6%, while the fission cross section σ_F was obtained from the ENDF/B-VII.0 database, with uncertainties ranging between 0.5% and 1% for the neutron energy domain of interest. The oxidation of the uranium sample used in the measurements leads to an additional 2% uncertainty on the self-absorption of the γ rays inside the sample. With statistical errors on the counting of the events by the detectors of 1% for the fission ionization chamber and, at best 1–2 % for the HPGe detectors, we are able to obtain final uncertainties of 3–5 % in the regions where sufficient statistics were available, i.e., where the γ production cross section and the incident neutron flux were sufficiently high to detect a large number of γ rays.

IV. RESULTS

The data presented in this work were obtained with a total beam time of 1466 hours.

A partial γ ray energy spectrum that was acquired with the ^{235}U sample is shown in Fig. 5, where proper time windows were chosen for radioactivity decay, for neutrons from 1 to 6 MeV representing the domain where the inelastic scattering reactions are strongest, and a window for neutrons of 8.5 to 16 MeV which corresponds to the domain of $(n, 2n)$ reactions. For the inelastic [Fig. 5(a)] and the $(n,2n)$ [Fig. 5(b)] domains, several γ-ray transitions, respectively in ^{235}U and ^{234}U, are identified. Those analyzed are mentioned in red and italic.

It is noteworthy that the spectrum observed contains a very large number of weak γ rays, which are due to the decay

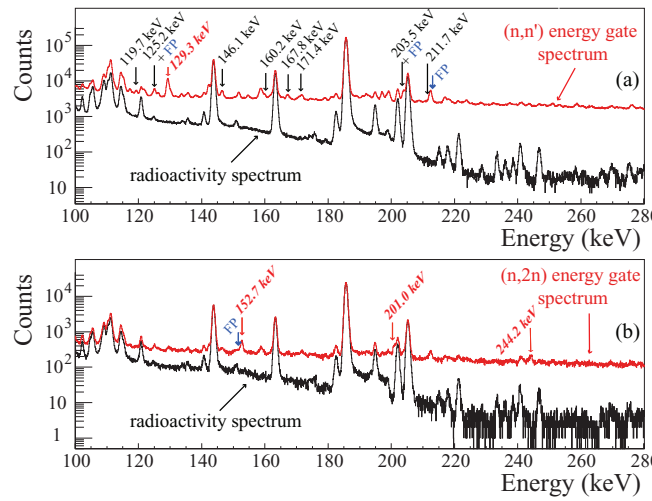

FIG. 5. (Color online) Partial γ energy spectrum gated on the (n, n') [(a), red] and the $(n, 2n)$ [(b), red] neutron energy domain compared to the radioactive decay γ-ray spectrum (black), acquired on the ^{235}U sample. The analyzed γ rays are shown in red and italic. γ rays from the decay of fission products are labeled by "FP" in blue.

TABLE IV. Identified γ energies of the ^{235}U energy spectra stemming from (n, n') and $(n, 2n)$ reactions. The rays for which results were obtained are shown in boldface.

E (keV)	Isotope	Initial state	Final state	γ multipolarity	Reaction type
119.7	^{235}U	$7/2^+$ ($E = 171.4$)	$5/2^+$ ($E = 51.7$)	$M1 + E2$	$(n, n'\gamma)$
125.0	^{235}U	$(1/2^-, 3/2^-)$ ($E = 990.2$)	$3/2^+$ ($E = 865.2$)	$E1$	$(n, n'\gamma)$
125.2	^{235}U	$7/2^+$ ($E = 171.4$)	$9/2^-$ ($E = 46.2$)	$E1$	$(n, n'\gamma)$
129.3	**^{235}U**	**$5/2^+$ ($E = 129.3$)**	**$7/2^-$ (GS)**	***E*1**	**$(n, n'\gamma)$**
146.1	^{235}U	$15/2^-$ ($E = 249.1$)	$11/2^-$ ($E = 103.0$)	$E2$	$(n, n'\gamma)$
152.7	**^{234}U**	**6^+ ($E = 296.1$)**	**4^+ ($E = 143.4$)**	***E*2**	**$(n, 2n\gamma)$**
160.2	^{235}U	$15/2^+$ ($E = 357.3$)	$13/2^+$ ($E = 294.7$)	$E2$	$(n, n'\gamma)$
167.8	^{235}U	$17/2^-$ ($E = 338.5$)	$13/2^-$ ($E = 170.7$)	$E2$	$(n, n'\gamma)$
171.4	^{235}U	$7/2^+$ ($E = 171.4$)	$7/2^-$ (GS)	$E1$	$(n, n'\gamma)$
201.0	**^{234}U**	**8^+ ($E = 497.0$)**	**6^+ ($E = 296.0$)**	***E*2**	**$(n, 2n\gamma)$**
203.5	^{235}U	$5/2^+$ ($E = 332.8$)	$5/2^+$ ($E = 129.3$)	$M1$	$(n, n'\gamma)$
211.7	^{235}U	$21/2^-$ ($E = 550.4$)	$17/2^-$ ($E = 338.7$)	$E2$	$(n, n'\gamma)$
244.2	**^{234}U**	**10^+ ($E = 741.2$)**	**8^+ ($E = 497.0$)**	***E*2**	**$(n, 2n\gamma)$**

of fission products created through (n, f) reactions (labeled by "FP" in blue in Fig. 5). As they are very numerous, it was not possible to identify all of them clearly. Moreover, these γ rays can become subject to superimposition with rays of interest, deteriorating the accuracy of the results or even making a proper analysis of several rays impossible. This is the case for a lot of transitions coming from (n, n') reactions. The identified γ energies stemming from (n, n') and $(n, 2n)$ reactions are shown in Table IV, in which the rays that were studied in this work are highlighted in boldface.

All cross sections obtained are compared to experimental data if they exist and to TALYS-1.2 calculations [10] for which several nuclear model inputs have been tested. In the literature, the cross sections are presented for the total deexcitation of the level; we have thus subtracted the internal conversion component with the internal conversion coefficients mentioned in the references. Moreover the TALYS-1.2 calculations have been performed only for the γ deexcitation of the level.

A. ^{235}U neutron inelastic scattering cross sections

Inelastic scattering reactions leave the target nucleus in an excited state if the neutron energy is higher than the reaction threshold. The deexciting of the nucleus to its ground state (GS) is realized by a γ-ray emission characteristic of the studied nucleus. This section studies the γ decays we observed.

There are several visible rays which are due to (n, n') reactions, as shown in Table IV, but unfortunately the spectra are strongly contaminated by γ radiation emitted by the fission products and by the background activity of the sample, so that finally only one γ ray could be analyzed: the 129.30 keV decay between the $\frac{5}{2}^+$ and $\frac{7}{2}^-$ states.

1. $\frac{5}{2}^+ \rightarrow \frac{7}{2}^-$ *(GS) transition in* ^{235}U

The decay of the $\frac{5}{2}^+$ state with energy 129.30 keV to the $\frac{7}{2}^-$ ground state is realized through the emission of a γ ray of 129.30 keV. As the transition goes to the ground state the energy threshold of the transition equals the energy of the emitted γ ray. The multipolarity of the transition is electric dipole ($E1$).

The γ ray of 129.30 keV in the energy spectra is mixed with another ray located around 130.2 keV. The latter one is present in the entire neutron domain and is probably emitted by a fission product after a neutron-induced fission reaction. Possible candidates for this ray include the 130.20 keV γ decay of ^{99}Zr or the 130.24 keV γ decay of ^{134}Cs. To disentangle both rays a double Gaussian fit has been applied. After this procedure a total yield of 636 787 counts is determined for the four detectors in the total integrated energy spectrum. These statistics allowed us to choose a binning leading to an evaluation of the cross section at 26 different neutron energy values. The analysis results of the total angle integrated cross section are shown in Fig. 6 and are compared to the only existing experimental data from Younes *et al.* [32].

From the threshold to the peak of the direct excitation of the $\frac{5}{2}^+$ state around 1 MeV the measured cross section agrees with the TALYS-1.2 pheno-cgmr (see the Discussion section) predictions [33], although a difference in the absolute values of almost 40% can be observed at 3 MeV. After this direct excitation component the shapes of both curves diverge. While the TALYS-1.2 code predicts a decrease of the γ production cross section, our measurements show an increasing hump before both curves describe the same final descending part.

The uncertainties of the experiment are below 4% for energies smaller than 7 MeV and increase up to 15% for the two high-energy points, since the statistics become weaker as the cross section gets lower. This corresponds to the best accuracy obtained on the measurement of the 129.30 keV γ decay of an inelastic scattering cross section.

B. ^{235}U$(n, 2n)$ reaction cross sections

After a $(n, 2n)$ reaction on ^{235}U, the residual ^{234}U nucleus is produced, and for energies above the threshold of this reaction the resulting ^{234}U is left in an excited state. The nucleus will decay to its ground state through the emission of characteristic γ rays. In this section the γ decays between the states 10^+

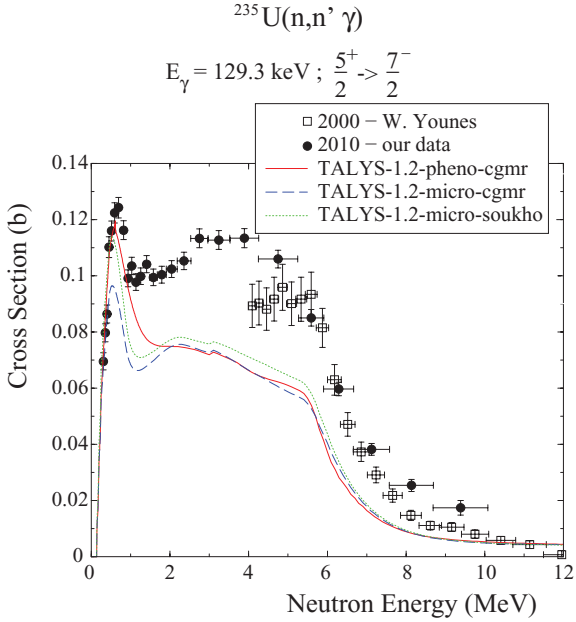

FIG. 6. (Color online) Total γ production cross section of the 129.30 keV transition from states $\frac{5}{2}^+ \rightarrow \frac{7}{2}^-$ due to a ^{235}U$(n, n')^{235}$U* reaction compared to TALYS-1.2 predictions and to other measurements. For this work, reported uncertainties are the combination of the statistical and systematic errors (see Sec. III F).

and 4^+ with energies of 152.72, 200.97, and 244.2 keV are analyzed. As the $2^+ \rightarrow 0^+$ γ transition ($E_\gamma = 43.5$ keV) is highly converted, it was not observed in this work. The $4^+ \rightarrow 2^+$ γ transition ($E_\gamma = 99.9$ keV) is mixed with a U x ray, but also with a transition in the decay daughter nucleus ^{231}Pa and probably also with a third one coming from an unidentified deexcitation (see Fig. 7). For these reasons, we have not considered this transition in the analysis.

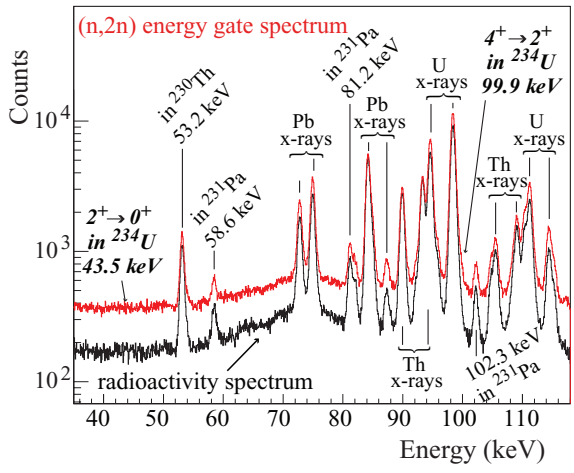

FIG. 7. (Color online) Low-energy part of the γ energy distribution gated on the $(n, 2n)$ (red) neutron energy domain compared to the radioactive decay γ-ray spectrum (black), acquired on the ^{235}U sample. This figure illustrates the extreme difficulty to extract accurate cross section values for low-lying states' deexcitations in ^{234}U.

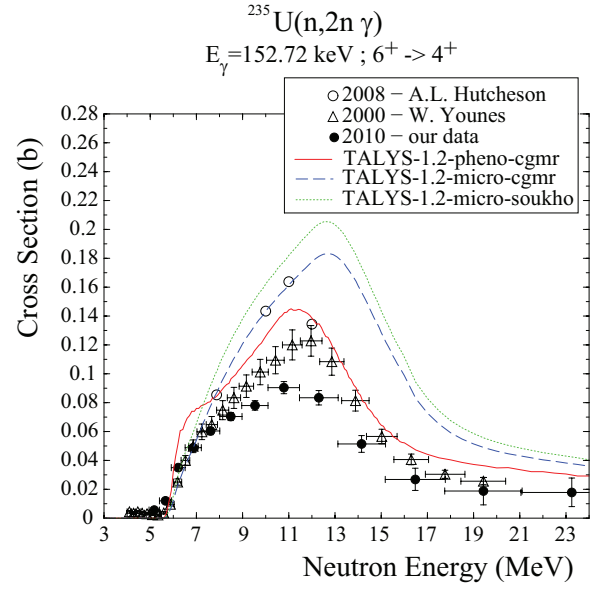

FIG. 8. (Color online) Total γ production cross section of the 152.72 keV transition from states $6^+ \rightarrow 4^+$ due to a ^{235}U$(n, 2n)^{234}$U* reaction compared to TALYS-1.2 predictions and other experimental measurements. For this work, reported uncertainties are the combination of the statistical and systematic errors (see Sec. III F).

1. $6^+ \rightarrow 4^+$ *transition in* ^{234}*U*

The decay between the states 6^+ ($E = 296.07$ keV) and 4^+ ($E = 143.35$ keV) in ^{234}U is realized through an emission of a γ ray with an energy of 152.72 keV. The threshold of this reaction corresponds to the neutron separation energy of ^{235}U and the required residual energy to leave the ^{234}U nucleus in the 6^+ excited state. For the emission of this γ ray the neutron threshold is 5.62 MeV. The multipolarity of the γ ray is $E2$.

Summing the four detectors, a total of 32 544 counts is obtained, which allowed us to select 13 neutron energy intervals to evaluate the reaction cross section. For this peak analysis, we have taken into account the contamination of a fission product decay (^{102}Zr) at 151.78 keV. The final total cross section for this transition is displayed in Fig. 8 together with the TALYS-1.2 code predictions and other measurements performed by Younes *et al.* [32] and from Hutcheson *et al.* [34].

One can observe that the results found by our measurements are lower by a factor 1.5 than the results predicted by TALYS-1.2 pheno-cgmr. Furthermore the TALYS-1.2 pheno-cgmr code seems to be in rather good agreement with the measured points of Younes *et al.*. The Hutcheson *et al.* data are close to the TALYS-1.2 micro-cgmr prediction except for the last experimental cross section at 12 MeV for which the cross section is significantly lower. When comparing our data points to the TALYS-1.2 γ production cross section, we can observe an excellent agreement in the shape of both curves, despite the fact that the theoretical predictions descend a little later than the experimental points. The uncertainties corresponding to the angle integrated cross sections are below 6% in the energy domain between 6 and 14 MeV. Near the threshold and the descending part of the cross section they are, however, higher, due to the low statistics in these ranges.

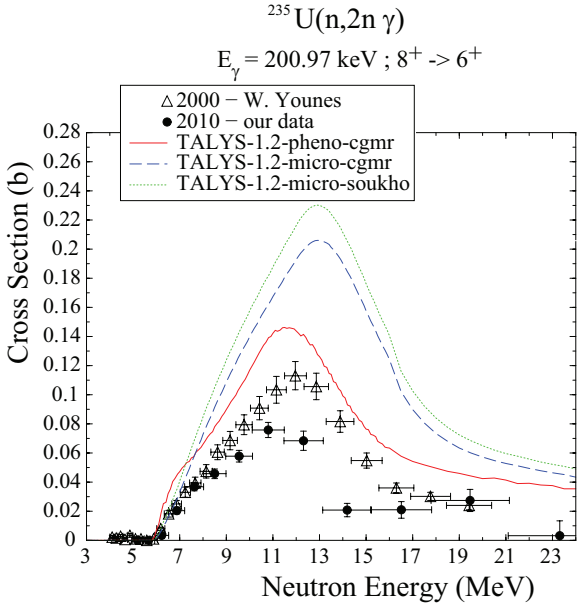

FIG. 9. (Color online) Total γ production cross section of the 200.97 keV transition from states $8^+ \rightarrow 6^+$ due to a ^{235}U$(n, 2n)^{234}$U* reaction compared to TALYS-1.2 predictions and prior measurements. For this work, reported uncertainties are the combination of the statistical and systematic errors (see Sec. III F).

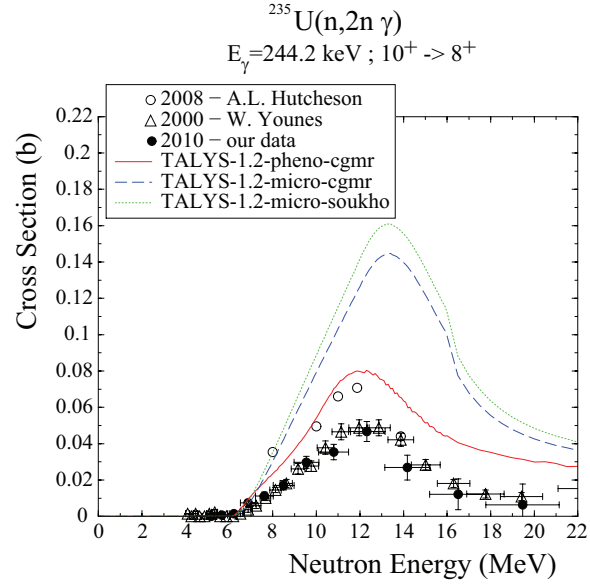

FIG. 10. (Color online) Total γ production cross section of the 244.2 keV transition from states $10^+ \rightarrow 8^+$ due to a ^{235}U$(n, 2n)^{234}$U* reaction compared to TALYS-1.2 predictions and other experimental measurements. For this work, reported uncertainties are the combination of the statistical and systematic errors (see Sec. III F).

2. $8^+ \rightarrow 6^+$ *transition in* ^{234}*U*

The transition between the 8^+ level at 497.04 keV and 6^+ level at 296.07 keV in the ^{234}U isotope can be observed by the detection of a γ ray of 200.97 keV. The reaction threshold for this $(n, 2n)$ reaction followed by a 200.97 keV γ decay is 5.82 MeV. The multipolarity of the transition is $E2$.

The 200.97 keV γ ray is mixed with the 202.11 keV ^{235}U decay γ ray in the energy spectra. For the grey and green detectors it was possible to distinguish both γ rays due to higher count rates and a better energy resolution. For the red detector the resolution was however not sufficient and the counting statistics of the blue detector were too weak to obtain reliable results in disentangling both contributions. The analysis of this transition is therefore based on the green and grey detectors only, for which a counting of 9374 was obtained enabling an evaluation of the cross section at 13 energy points. The angle integrated cross section is shown in Fig. 9.

In this case, our experimental data are also lower by a factor 1.3 than those measured by Younes *et al*. Here, we can observe that the shape of the cross section curve is very close to the one predicted by TALYS-1.2 pheno-cgmr, although its absolute value is approximately a factor 1.9 lower, which is close to the factor obtained for the 152.72 keV transition cross section.

Analogously as for the previous transition, the errors are below 7% in the energy domain from 6 to 12 MeV, and higher in the low- and high-energy regions, where the γ-ray yield is reduced due to the lower transition probability.

3. $10^+ \rightarrow 8^+$ *transition in* ^{234}*U*

The emission of a 244.2 keV γ ray is related to the transition from the 10^+ to 8^+ states of energies 741.20 and 497.04 keV respectively in ^{234}U. The threshold for such a γ ray to be observable after an $(n, 2n)$ reaction is 6.06 MeV. This transition is an electric transition of second order ($E2$).

A total number of 3796 counts was obtained for this γ radiation on the green and grey detectors but the statistics of the red and blue detector were too low to deliver acceptable results. The cross section has been evaluated at 12 neutron energy points as shown for the total angle-integrated cross section in Fig. 10.

In this case, our new measurements are in very good agreement with those of Younes *et al*. while the difference with the TALYS-1.2 pheno-cgmr is now of the order of 1.5. As for the $6^+ \rightarrow 4^+$ γ transition, the Hutcheson *et al*. data are higher and the maximum of the cross section seems to be shifted to lower neutron energies.

For this transition, the accuracy reaches 11% in the energy domain between 9 and 14 MeV.

V. DISCUSSION

The comparison of the experimental $(n, xn\gamma)$ cross sections of ^{235}U with TALYS-1.2 predictions displays rather significant differences depending on the number of emitted neutrons. Whereas the situation is not so bad for inelastic cross sections up to 8 MeV, the experimental values strongly differ from the calculations for $(n, 2n\gamma)$ cross sections.

In order to study the sensitivity of the model predictions to the nuclear model inputs, we have tried to use several optical model potentials as well as several types of level densities and γ-ray strength function models. To be more explicit, three types of calculations have been performed: The first type of approach (pheno-cgmr) is obtained using sets of fine tuned phenomenological inputs together with a

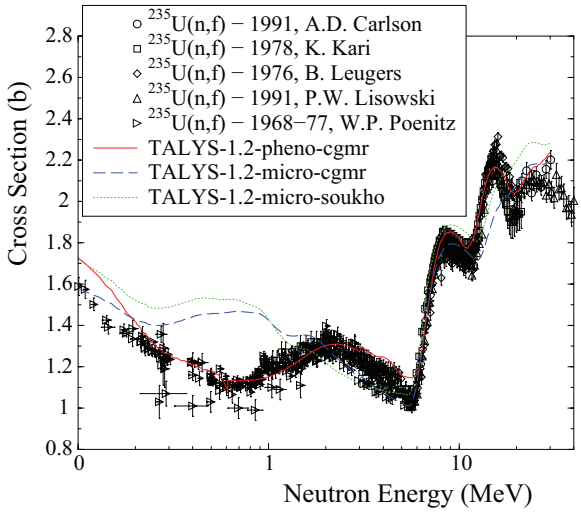

FIG. 11. (Color online) Total ^{235}U(n, f) cross section computed by TALYS-1.2 and compared to evaluated database values.

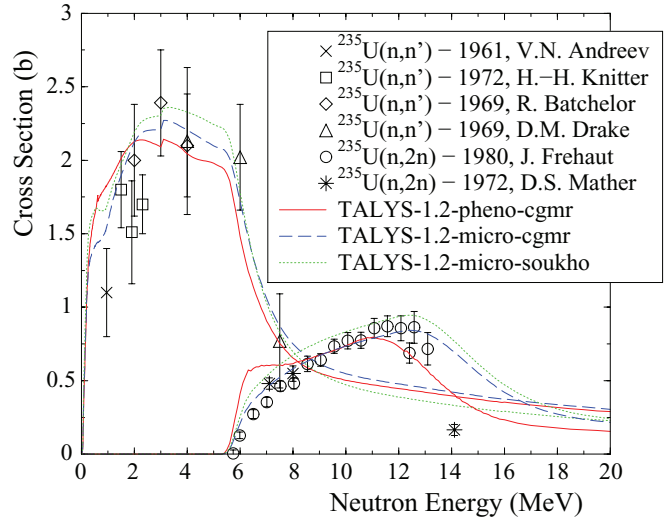

FIG. 12. (Color online) Total ^{235}U(n, n') and total ^{235}U$(n, 2n)$ cross section computed by TALYS-1.2 and compared to evaluated database values.

specific global optical model potential (cgmr) [35]. The second one (micro-soukho) corresponds to the microscopic inputs of Ref. [36] using the default phenomenological optical model potential of Soukhovitskii [37] implemented in TALYS-1.2 for actinides. Finally, in order to study the impact of the optical model potential on the predictions, we have combined in a third approach (micro-cgmr) the microscopic inputs with the cgmr optical model. As can be seen, whatever the approach, the situation remains globally the same, even if the pheno-cgmr combination provides the best results, in particular for the shapes of the $(n, 2n\gamma)$ channels. The much stronger overestimation of the $(n, 2n\gamma)$ cross sections observed using the microscopic inputs is a direct consequence of the lower fission cross section obtained with this set of input in the 10–15 MeV range (cf. Fig. 11).

Such a disagreement can be due to several reasons, among which the most important might be the very approximative description of preequilibrium reactions. Indeed, the low-energy reactions, typically below 8 MeV, are dominated by the well modeled compound nucleus reaction mechanism while the preequilibrium mechanism begins to play a significant role in the region where $(n, 2n)$ cross sections occur. In TALYS-1.2, preequilibrium reactions are modeled using the semi-classical *exciton model*, for which spin distributions are probably too crudely described. The impact of a too rough description has already been studied by Kawano *et al.* [38] on inelastic cross sections of ^{193}Ir and it has been shown that spin distributions obtained using the quantum mechanical Feshbach-Kerman-Koonin (FKK) [39] approach are peaked at much lower spin values than those used in the *exciton model*, thus enhancing the probability of γ decay to low spin states with respect to the semiclassical case. In the current case, a similar study would be of particular interest to check if a better agreement would then be obtained.

It is also noteworthy to mention that the branching ratios of the different excitation levels are of very high importance for the absolute values of the measured γ production cross sections, and that level densities can lead to variations in the competition between inelastic and $(n, 2n)$ cross sections. All these parameters are connected and thus crucial to obtain correct results. However, by looking carefully at the level structure database of TALYS-1.2, we have not found any particular problem or source of error in the branching ratios which could explain the strong disagreement observed for the $(n, 2n\gamma)$ channels. The same remark holds for the level densities since we have employed on one hand a purely phenomenological approach and on the other hand the nonstatistical approach of Ref. [40] without noticing an improvement in the cross section description. Another source of uncertainty in the predictions could be due to the model employed to describe internal conversion in competition with the γ decay.

The main differences between the various approaches are mainly due, as mentioned above, to a different description of the competition between fission and (n, xn) channels. If this competition is not well under control, it is clear that (n, xn) reactions might not be well reproduced and consequently the $(n, xn\gamma)$ reactions also. Such a situation is encountered both for the micro-shoukho and the micro-cgmr choices, as already explained before. In the case of the pheno-cgmr approach, as shown in Figs. 11 and 12, this is not a possible explanation since (n, f), (n, n') and $(n, 2n)$ channels are rather well described by the model predictions.

VI. CONCLUSIONS

In this work, several $(n, xn\gamma)$ reaction cross sections were measured at a precision never reached before. The results of this measurement can be used to work out a better parametrization of the TALYS-1.2 code. The difference on the ^{235}U$(n, 2n)$ reaction cross section values could be caused by the fact of neglecting the spin distributions in the preequilibrium model calculation of TALYS-1.2. Wrong branching ratios of the different decay channels in ^{235}U, missing precision on the nuclear level densities, as well as a bad parametrization of the neutron-induced fission cross section can lead to further

differences. With our measurements these parameters can be optimized and the reliability of the code can be improved.

The work on the improvement of the precision permits the experimental setup to study $(n, xn\gamma)$ reactions at accuracies of 3% presuming long enough experimental runs, reducing the counting uncertainties to below 1%. This setup can now be used to measure reactions such as the inelastic scattering on ^{238}U, for which a high priority is assigned [5].

A next step in the measurement is determination of $(n, xn\gamma)$ reaction cross sections on enriched isotopes of tungsten (^{182}W, ^{183}W, ^{184}W, and ^{186}W), for which the comparison to model codes is easier as they are not fissionable and hence do not need the fission decay channel to be taken into account.

ACKNOWLEDGMENTS

The authors thank the team of the GELINA facility for the preparation of the neutron beam and for their strong support day after day. They also thank, R. Nolte, M. Mosconi and S. Röttger [Physikalisch-Technische Bundesanstalt (PTB)] for their help concerning the characterization and calibration of the fission chamber. This work was partially supported by the European Commission within the Sixth Framework Programme through I3-EFNUDAT (EURATOM Contract No. 036434) and NUDAME (Contract No. FP6-516487), and within the Seventh Framework Programme through EUFRAT (EURATOM Contract No. FP7-211499).

[1] The Generation IV International Forum, http://www.gen-4.org/.
[2] G. Aliberti, G. Palmiotti, M. Salvatores, and C. G. Stenberg, Nucl. Sci. Eng. **146**, 13 (2004).
[3] M. Salvatores, G. Aliberti, G. Palmiotti, D. Rochman, P. Oblozinsky, M. Hermann, P. Talou, T. Kawano, L. Leal, A. Koning *et al.*, in *Proceedings of the International Conference on Nuclear Data for Science and Technology–ND2007* (EDP Sciences, Paris, France, 2008), pp. 879–882.
[4] M. Salvatores, G. Aliberti, and G. Palmiotti, in *Proceedings of the International Conference on Nuclear Data for Science and Technology–ND2007* (EDP Sciences, Paris, France, 2008), pp. 883–886.
[5] OECD/NEA Nuclear Data High Priority Request List, http://www.nea.fr/dbdata/hprl/.
[6] F. Voss, S. Cierjacks, D. Erbe, and G. Schmatz, Technical Report No. 2379, Kernforschungszentrum Karlsruhe, 1976 (unpublished).
[7] D. C. Larson and J. K. Dickens, Phys. Rev. C **39**, 1736 (1989).
[8] H. Vonach, A. Pavlik, M. B. Chadwick, R. C. Haight, R. O. Nelson, S. A. Wender, and P. G. Young, Phys. Rev. C **50**, 1952 (1994).
[9] L. A. Bernstein, J. A. Becker, P. E. Garrett, W. Younes, D. P. McNabb, D. E. Archer, C. A. McGrath, H. Chen, W. E. Ormand, M. A. Stoyer *et al.*, Phys. Rev. C **65**, 021601 (2002).
[10] A. Koning, S. Hilaire, and M. Duijvestijn, in *Proceedings of the International Conference on Nuclear Data for Science and Technology–ND2007* (EDP Sciences, Paris, France, 2008), pp. 211–214.
[11] M. Flaska, A. Borella, D. Lathouwers, L. C. Mihailescu, W. Mondelaers, A. J. M. Plompen, H. van Dam, and T. H. J. J. van der Hagen, Nucl. Instrum. Methods Phys. Res., Sect. A **531**, 392 (2004).
[12] D. Ene, C. Borcea, S. Kopecky, W. Mondelaers, A. Negret, and A. Plompen, Nucl. Instrum. Methods Phys. Res., Sect. A **618**, 54 (2010).
[13] D. Tronc, J. Salom, and K. Bckhoff, Nucl. Instrum. Methods Phys. Res., Sect. A **228**, 217 (1985).
[14] J. Allison *et al.*, Nucl. Instrum. Methods Phys. Res., Sect. A **506**, 250 (2003).
[15] D. Deleanu, C. Borcea, P. Dessagne, M. Kerveno, A. Negret, A. J. M. Plompen, and J. C. Thiry, Nucl. Instrum. Methods Phys. Res., Sect. A **624**, 130 (2010).
[16] G. Kerckhofs, J. Schrooten, T. Van Cleynenbreugel, S. V. Lomov, and M. Wevers, Rev. Sci. Instrum. **79**, 013711 (2008).
[17] MCNPX, http://mcnpx.lanl.gov/.
[18] J. C. Thiry, C. Borcea, P. Dessagne, J. C. Drohé, E. Jericha, H. Karam, M. Kerveno, A. J. Koning, A. L. Negret, A. Pavlik *et al.*, in *Proceedings of NEMEA-6, Nuclear Measurements, Evaluations and Applications, Krakow, Poland, 2010* (OECD, Paris, France, 2011), http://www.oecd-nea.org/science/wpec/nemea6/.
[19] J. C. Thiry, Ph.D. thesis, University of Strasbourg, 2010.
[20] C. Budtz-Jørgensen, H. Knitter, and G. Bortels, Nucl. Instrum. Methods Phys. Res., Sect. A **236**, 630 (1985).
[21] G. W. Carlson, Nucl. Instrum. Methods Phys. Res. **119**, 97 (1974).
[22] A. J. M. Plompen, C. Borcea, D. Deleanu, P. Dessagne, M. Kerveno, M. Mosconi, N. Nankov, A. Negret, R. Nolte, C. Rouki *et al.*, in *Proceedings of the International Conference on Nuclear Data for Science and Technology–ND2010*, Jeju Island, Korea, 2011 [J. Korean Phys. Soc. **59**, 1880 (2011)].
[23] M. Mosconi, Ph. Dessagne, M. Kerveno, R. Nolte, A. J. M. Plompen, C. Rouki, and J. C. Thiry, in *Proceedings of the Final Scientific EFNUDAT Workshop* (CERN, Geneva, Switzerland, 2010), pp. 105–111.
[24] T. Gouder, C. Colmenares, J. Naegele, and J. Verbist, Surf. Sci. **235**, 280 (1990).
[25] L. Arnold, R. Baumann, E. Chambit, M. Filliger, C. Fuchs, C. Kieber, D. Klein, P. Medina, C. Parisel, M. Richer, C. Santos, and C. Weber, in *Proceedings of 14th IEEE-NPSS Real Time Conference* (Alba Nova University Centre, Stockholm, Sweden, 2005), pp. 265–269.
[26] V. T. Jordanov and G. F. Knoll, Nucl. Instrum. Methods Phys. Res., Sect. A **345**, 337 (1994).
[27] D. C. Radford, Oak Ridge National Laboratory Physics Division report (unpublished), http://radware.phy.ornl.gov/gf3/gf3.html.
[28] C. R. Brune, Nucl. Instrum. Methods Phys. Res., Sect. A **493**, 106 (2002).
[29] E. Sheldon and D. Van Patter, Rev. Mod. Phys. **38**, 143 (1966).
[30] R. D. Gill, *Gamma-ray Angular Correlations and Distributions* (Academic, London, 1975).
[31] L. Mihailescu, L. Oláh, C. Borcea, and A. J. M. Plompen, Nucl. Instrum. Methods Phys. Res., Sect. A **531**, 375 (2004).
[32] W. Younes, J. Becker, L. Bernstein, P. Garrett, C. Mc Grath, D. McNabb, R. Nelson, M. Devlin, N. Fotiades, and G. Johns, Lawrence Livermore National Laboratory Technical Report No. UCRL-ID-140313 (unpublished).
[33] P. Romain (private communication).
[34] A. Hutcheson, Ph.D. thesis, Duke University, 2008.

[35] C. Sage, V. Semkova, O. Bouland, P. Dessagne, A. Fernandez, F. Gunsing, C. Nästren, G. Noguère, H. Ottmar, A. J. M. Plompen *et al*., Phys. Rev. C **81** 064604 (2010).
[36] S. Goriely, S. Hilaire, A. J. Koning, and R. Capote, Phys. Rev. C **83**, 034601 (2011).
[37] E. S. Soukhovitskii, S. Chiba, J.-Y. Lee, O. Iwamoto, and T. Fukahori, J. Phys. G **30**, 905 (2004).
[38] T. Kawano, P. Talou, and M. B. Chadwick, Nucl. Instrum. Methods Phys. Res., Sect. A **562**, 774 (2006).
[39] H. Feshbach, A. Kerman, and S. Koonin, Ann. Phys. (NY) **125**, 429 (1980).
[40] S. Goriely, S. Hilaire, and A. J. Koning, Phys. Rev. C **78**, 064307 (2008).